

# Preliminary Study on Fe(III) Detection Using Nitrogen-Doped Carbon Quantum Dots via HSV-Based Smartphone Fluorescence Analysis

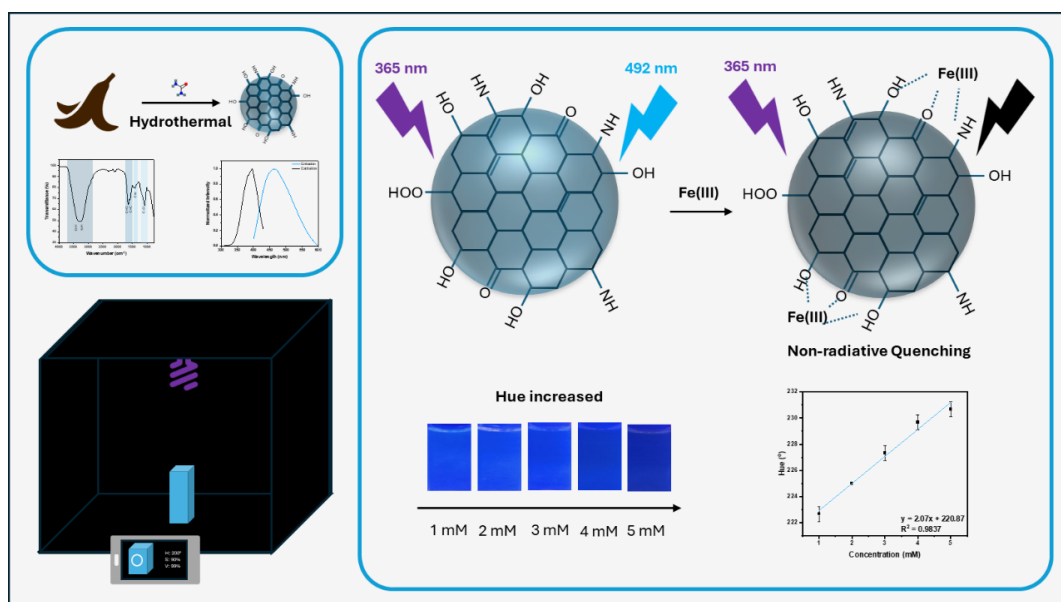
Erika Agustina, Wulan Amalia Mustika Damayanti, Abdul Aji, M Alvien Ghifari\*

Department of Chemistry, Faculty of Science, Institut Teknologi Sumatera, Jalan Terusan Ryacudu, Lampung Selatan, Lampung, 35365 Indonesia

\* corresponding author: [m.ghifari@ki.itera.ac.id](mailto:m.ghifari@ki.itera.ac.id)

DOI: 10.20885/ijca.vol8.iss2.art3

## GRAPHICAL ABSTRACT



## ARTICLE INFO

Received : 09 July 2025

Revised : 15 August 2025

Published : 29 September 2025

Keywords : N-CQDs, banana peel, fluorescence, HSV, Fe(III)

## ABSTRACT

This study successfully synthesized nitrogen-doped carbon quantum dots (N-CQDs) from banana peel waste via a hydrothermal method using urea as the nitrogen source. FTIR and optical characterization confirmed the presence of hydroxyl, carbonyl, and amine functional groups, along with distinct photophysical features, including an absorption peak at 304 nm, excitation at 392 nm, and blue fluorescence emission at 465 nm. Upon Fe(III) exposure, the N-CQDs exhibited selective fluorescence quenching and a measurable hue (H) value shift. A linear relationship was observed between hue and Fe(III) concentration in the 1-5 mM range ( $R^2 = 0.9822$ ). The limit of detection (LOD) and limit of quantification (LOQ) were estimated at 0.948 mM and 2.875 mM, respectively. These findings demonstrate the potential of banana peel-derived N-CQDs as a low-cost, environmentally friendly, and smartphone-compatible fluorescence probe for Fe(III) detection in aqueous environments.

## 1. INTRODUCTION

Heavy metal ion contamination poses a significant threat due to its toxicity and persistence in aquatic systems [1], [2], [3]. Among these, Fe(III) is one of the most prevalent pollutants, often originating from industrial wastewater [4], [5], [6]. Prolonged exposure to Fe(III)-contaminated water can lead to serious health issues, including cancer, kidney failure, and neurological disorders [2]. Therefore, developing simple, sensitive, and cost-effective methods for Fe(III) detection is essential.

Conventional techniques such as atomic absorption spectroscopy (AAS), atomic emission spectroscopy (AES), and inductively coupled plasma atomic emission spectroscopy (ICP-AES) are widely employed for metal ion analysis [7]. However, these methods often require expensive instrumentation, complex sample preparation, and trained personnel, making them less suitable for rapid or field-based monitoring [8]. In contrast, optical sensing, particularly fluorescence-based methods, has emerged as a promising alternative due to its simplicity and potential for real-time analysis [7], [9], [10].

Fluorescence quenching, caused by interactions between fluorescent probes and analytes, provides a sensitive mechanism for detection [11], [12]. Recently, smartphone-integrated platforms utilizing HSV (hue, saturation, value) color space analysis have gained attention for their accessibility and ability to quantify subtle fluorescence changes, especially when visual observation alone is insufficient [13], [14], [15], [16], [17].

Carbon quantum dots (CQDs) are a class of fluorescent nanomaterials widely studied for optical sensing applications due to their excellent water solubility, photostability, tunable emission, and low toxicity [18]. Their performance can be further enhanced by heteroatom doping, particularly with nitrogen, which improves quantum yield and introduces functional groups favorable for analyte interaction [19], [20], [21], [22], [23]. Reported quantum yields of nitrogen-doped CQDs (N-CQDs) vary from 31% to over 50%, depending on the nitrogen source used, such as ethylenediamine, urea, or ammonia [24], [25].

Various methods have been developed for N-CQDs synthesis, including microwave-assisted, hydrothermal, and solvothermal approaches [23], [24], [26], [27], [28], [29]. Among them, hydrothermal synthesis is particularly attractive due to its simplicity, low cost, and eco-friendly process. Banana peel, rich in carbon and protein, has been explored as a sustainable precursor for CQD synthesis [30].

While N-CQDs derived from banana peels and their application in Fe(III) detection have been previously reported [19], [20], [21], [22], [23], this study introduces a novel approach by employing the hue (H) parameter from the HSV color space as the primary analytical signal in a smartphone-based fluorescence detection system. Unlike conventional intensity-based fluorescence detection, the hue approach provides a visually interpretable and equipment-free quantification strategy, enhancing accessibility and simplicity of applications. This work aims to develop a low-cost, eco-friendly, and portable optical sensor for Fe(III) detection in aqueous environments.

## 2. EXPERIMENTAL METHODS

### 2.1. N-CQDs synthesis

Banana peel from a local market was dried, ground, and sieved (50 mesh). A total of 2 g of the banana peel powder was mixed with 0.15 g of urea (Merck) in 40 mL of deionized water and stirred until a homogeneous suspension was obtained. The mixture was transferred into a Teflon-lined stainless-steel autoclave and subjected to hydrothermal treatment at 180 °C for 18 hours in an oven. After cooling to room temperature, the resulting mixture was filtered to separate the liquid phase (N-CQDs suspension) from residual solids. The filtrate was centrifuged at 3000 rpm for 10 minutes to remove remaining particulates. The clear supernatant, containing the N-CQDs, was collected for further characterization.

### 2.2. Metal ion detection

A detection test was performed against various metal ions to evaluate the fluorescence response of the nitrogen-doped carbon quantum dots (N-CQDs). A total of 2.5 mL of the N-CQD suspension was mixed with 0.5 mL of 5 mM metal ion solutions, including Ni(II), Cu(II), Fe(II), Co(II), Mn(II), Pb(II), and Fe(III) (Merck). The resulting mixtures were thoroughly mixed and

exposed to a 365 nm UV lamp to induce photoluminescence. The fluorescence emission of each sample was visually monitored and digitally captured using a Samsung M20. Images were then analyzed using the HSV Color Grab application to extract color parameters (Hue, Saturation, and Value), enabling quantitative assessment of the optical response toward each metal ion.

All fluorescence images were captured using the same smartphone camera model under fixed settings to prevent variability due to smartphone camera quality. To ensure reproducibility and minimize ambient light interference, imaging was performed in a custom-built light box equipped with a 365 nm UV lamp and black matte interior, as shown in Figure 1. This setup provided uniform illumination and minimized reflection or shadow artifacts. Three replicate images were analyzed for each condition to assess measurement consistency.

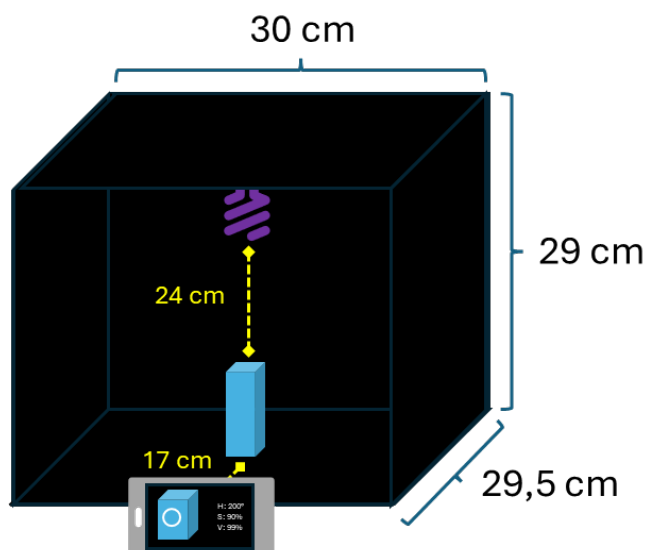


Figure 1. Schematic illustration of the custom-built light box used to standardize lighting conditions during smartphone-based image acquisition.

### 2.3. Characterization

Fourier-transform infrared (FTIR) spectroscopy was conducted using an Agilent Cary 680 FTIR spectrometer to identify the surface functional groups on the N-CQDs. The FTIR measurements were carried out in the 400-4000  $\text{cm}^{-1}$  spectral range. The optical properties of the nitrogen-doped carbon quantum dots (N-CQDs) were investigated using a UV-Vis spectrophotometer (Thermo Scientific Genesys 150). The absorption spectrum was recorded in the 200-800 nm wavelength range to determine the N-CQD suspension's maximum absorption wavelength. Fluorescence characterization was performed using a Horiba FluoroMax Hybrid spectrofluorometer to determine both the excitation and emission wavelengths of the N-CQDs. The excitation spectra were recorded between 300 and 400 nm, while the emission spectra were collected in the 300 and 600 nm range.

## 3. RESULTS AND DISCUSSIONS

### 3.1. FTIR Analysis

FTIR spectroscopy was employed to investigate the surface functional groups of N-CQDs synthesized from banana peel using urea as a nitrogen source. As shown in Figure 2, bands at 3332 and 3265  $\text{cm}^{-1}$  are observed, corresponding to the stretching vibrations of O-H and N-H groups [24], [31]. These hydrophilic groups are beneficial to enhance the aqueous solubility of N-CQDs, facilitating uniform dispersion during applications [32], [33], and also serve as active sites for metal ions through coordination complex formation [34].

Distinct bands observed around 1640 and 1580  $\text{cm}^{-1}$  are attributed to C=O and C=C stretching vibrations, indicating the presence of carbonyl functionalities and partial graphitization [34]. The band at 1416  $\text{cm}^{-1}$  is assigned to C-N stretching vibrations, confirming successful nitrogen incorporation on the CQD surface during urea-assisted doping [31]. Furthermore, the strong band at

1073  $\text{cm}^{-1}$  corresponds to C-O stretching, evidencing the presence of oxygen-containing functional groups [24]. These findings align with the report by Atchudan et al, who observed similar -OH, and in ammonia-derived N-CQDs from banana peel [31]. Overall, the FTIR results confirm that the synthesized N-CQDs possess a rich variety of surface functional groups beneficial for aqueous dispersion and metal ion sensing.

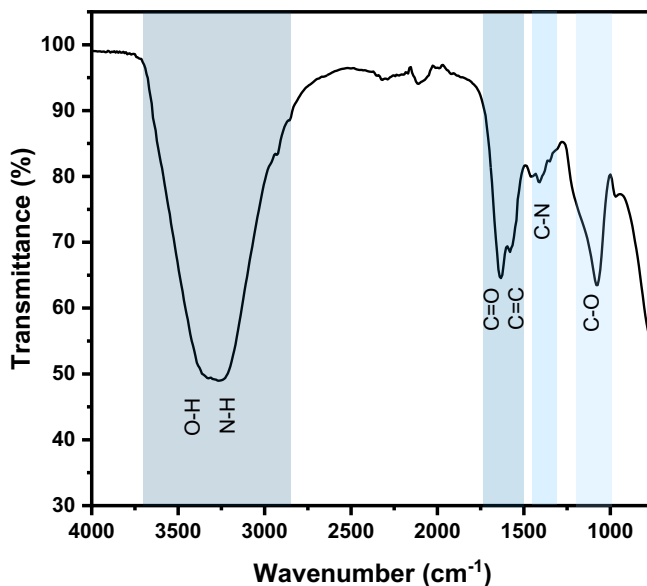


Figure 2. FTIR spectrum of nitrogen-doped carbon quantum dots (N-CQDs).

## 2.4. Optical Properties

The optical properties of the synthesized nitrogen-doped carbon quantum dots (N-CQDs) were investigated using UV-Vis absorption spectroscopy and fluorescence spectroscopy. As shown in Figure 3 (a), a strong absorption peak appears at 304 nm, corresponding to  $n-\pi^*$  transition associated with C=O groups on the N-CQDs surface [35]. This observation agrees with the FTIR results, confirming the presence of C=O groups contributing to the optical absorption behavior.

Fluorescence characterization in Figure 3 (b) revealed that the N-CQDs exhibit blue emission centered at 465 nm when excited at 392 nm. This emission arises from the relaxation process following photon absorption, wherein electrons are promoted to higher excited states upon UV irradiation and subsequently relax via non-radiative pathways before returning to the ground state by photon emission [36]. Notably, the emission wavelength is red-shifted relative to the excitation wavelength, a phenomenon known as the Stokes shift. Consistent with our findings, Shen et al. reported that nitrogen-doped CQDs exhibited a notable Stokes shift, with an excitation peak at 320 nm and an emission peak at 460 nm [37]. The blue emission of the synthesized N-CQDs highlights their potential as optical probes for metal ion detection.

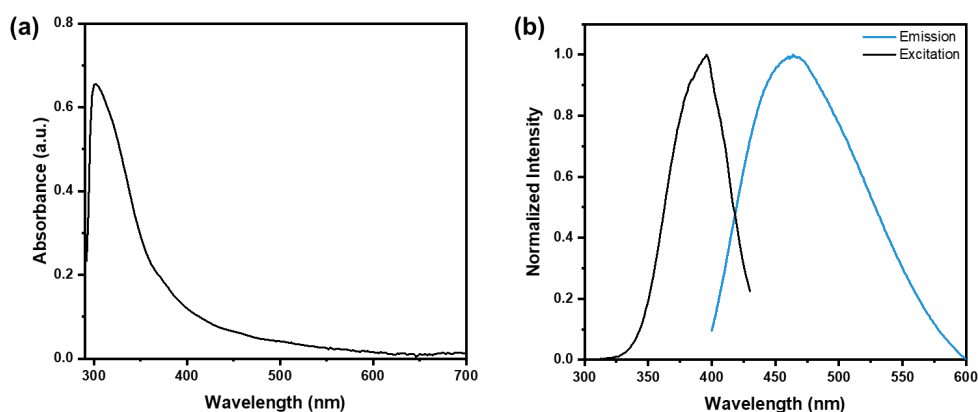


Figure 3. (a) UV-Vis absorbance spectrum, (b) excitation and emission spectra of N-CQDs.

2.5. Metal ion detection

While smartphone-based HSV analysis offers a low-cost and accessible approach to fluorescence sensing, variations in camera sensor specifications and ambient lighting conditions can introduce inconsistencies in color capture. Therefore, standardizing the imaging environment is critical to ensure reproducible and reliable measurements. This study acquired all fluorescence images inside a custom-built enclosed light box equipped with a fixed 365 nm UV light source. This setup provided uniform illumination and minimized external light interference, allowing for consistent HSV analysis across all measurements.

The fluorescence response of N-CQDs to various metal ions (Ni(II), Cu(II), Fe(II) Co(II), Mn(II), Pb(II), and Fe(III); 5 mM) was evaluated under 365 nm UV illumination using smartphone-assisted HSV (hue, saturation, value) analysis. Each measurement was performed in triplicate (n = 3) to ensure reproducibility. As summarized in Table 1, the N-CQDs displayed bright blue emission without metal ions. Only Fe(III) caused a significant color change from bright blue to bluish-black among all tested ions, indicating selective quenching.

Figure 4(a)-(c) plots the HSV parameters following ion exposure. The hue (H) value of pristine N-CQDs was  $201.67 \pm 0.54^\circ$ , consistent with blue emission. After exposure to other metal ions, H values showed a slight change ( $205\text{--}209.33^\circ$ ). However, Fe(III) induced a substantial shift to  $227.33 \pm 1.69^\circ$ , confirming a notable spectral change (Figure 4(a)).

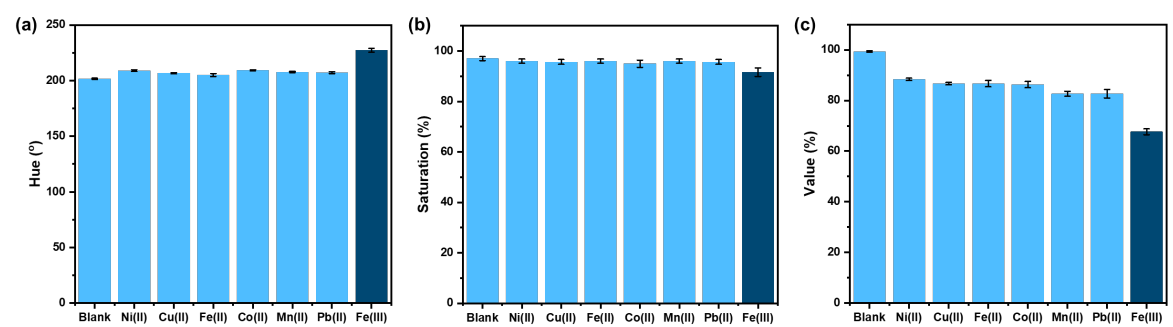










Figure 4. (a) Hue (H), (b) Saturation (S), and (c) Value (V) of N-CQDs fluorescence after metal ion addition.

Similarly, the saturation (S) parameter remained stable (95–97%) for most ions but decreased to  $91.67 \pm 1.69\%$  with Fe(III) (Fig. 4(b)), indicating a reduction in emission purity. The brightness or value (V) parameter dropped significantly from  $99.33 \pm 0.27\%$  to  $67.67 \pm 1.15\%$  with Fe(III) addition. At the same time, other ions caused only minor alterations (Fig. 4(c)). These results demonstrate the high selectivity of N-CQDs toward Fe(III) ions.

TABLE I. HSV (Hue, Saturation, Value) values of N-CQDs after exposure to various metal ions (5 mM) (n = 3).

Metal ion	Digital image		H (°)	S(%)	V(%)
	Before	After			
Ni(II)			209 ± 0.81	96 ± 0.81	88.33 ± 0.47
Cu(II)			206.67 ± 0.47	95.67 ± 0.94	86.67 ± 0.47
Fe(II)			205 ± 1.41	96 ± 0.81	86.67 ± 1.24

Co(II)			$209.33 \pm 0.47$	$95 \pm 1.41$	$85.67 \pm 1.24$
Mn(II)			$207.67 \pm 0.47$	$96 \pm 0.81$	$82.67 \pm 0.94$
Pb(II)			$207 \pm 0.81$	$95.67 \pm 0.94$	$82.67 \pm 1.69$
Fe(III)			$227.33 \pm 1.69$	$91.67 \pm 1.69$	$67.67 \pm 1.15$

The quenching mechanism is likely attributed to static quenching due to the formation of surface complexes between Fe(III) and functional groups (-OH, -NH, C=O) on the N-CQDs [38], [39], [40]. Fe(III), as a strong electron acceptor with vacant d-orbitals, facilitates non-radiative electron transfer from excited CQDs to the metal ion, leading to fluorescence quenching [34], [41]. Additionally, Fe(III), classified as a hard Lewis acid, preferentially binds to the hydroxyl groups (hard bases) on the CQD surface [42]. In contrast, other metal ions exhibited minimal quenching due to their weaker affinity and lower electron-accepting capability [43].

## 2.6. Analytical Performance

To assess the quantitative potential of N-CQDs for Fe(III) detection, a linearity test was conducted by varying Fe(III) concentrations from 1 to 5 mM and analyzing the resulting fluorescence emission via HSV color parameters. Each concentration point was measured in triplicate ( $n = 3$ ) to ensure statistical reliability. The results are presented in Table 2 and Fig. 5 (a)–(c).

The hue (H) value showed a substantial linear increase with Fe(III) concentration (Figure 5(a)), shifting emission from blue to bluish-black. The regression equation was  $y = 2.07x + 220.87$  with  $R^2 = 0.9837$ , indicating a high correlation. Saturation (S), however, exhibited a non-linear response, peaking at low concentrations and declining at higher ones (Figure 5(b)), with a weak correlation ( $R^2 = 0.6173$ ). Brightness (V) values decreased progressively with increasing Fe(III) concentration (Fig. 5(c)), with a regression of  $y = -7.03x + 103.91$  and  $R^2 = 0.9104$ , suggesting it as another useful quantification parameter. Hue (H) demonstrated the most consistent and significant correlation with Fe(III) concentration among the HSV parameters, exhibiting minimal deviation across replicates. In contrast, saturation (S) showed a non-monotonic response, and value (V) was more sensitive to variations in background illumination, thereby reducing their reliability as analytical indicators [44]. H was therefore selected as the primary analytical parameter due to its higher sensitivity and linearity.

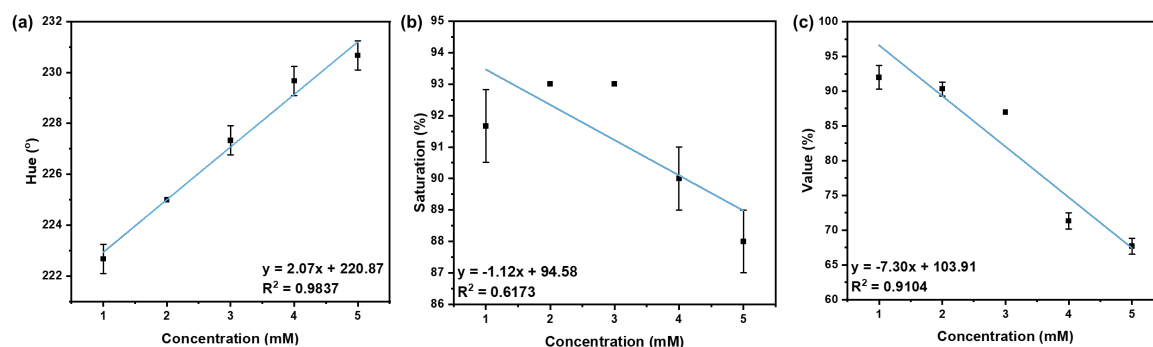



Figure 5. Linear relationship between Fe(III) concentration and (a) hue (H), (b) saturation (S), and (c) value (V) of N-CQDs.



TABLE II. HSV (Hue, Saturation, Value) values of N-CQDs after exposure to various concentrations of Fe(III) (n = 3).

Fe(III) concentration (mM)	Digital image	H (°)	S (%)	V (%)
1		222.67 ± 0.57	91.67 ± 1.15	92 ± 1.73
2		225 ± 0	93 ± 0	90.33 ± 1
3		227.33 ± 0.57	93 ± 0	87 ± 0
4		229.67 ± 0.57	90 ± 1	71.33 ± 1.15
5		230.67 ± 0.57	88 ± 1	67.67 ± 1.15

LoD and LoQ were calculated using the formulas  $3.3\sigma/m$  and  $10\sigma/m$ , where  $\sigma$  represents the standard deviation of the response and  $m$  is the slope of the calibration curve [45]. Using a standard deviation of 0.708 and a slope of 2.07 obtained from the hue (H) calibration curve, the LoD and LoQ were estimated to be 0.948 mM and 2.875 mM, respectively. These values are relatively high compared to the permissible Fe(III) concentration in iron mining wastewater, which is 5 mg/L (equivalent to ~0.089 mM), as specified by the Indonesian Ministry of Environment. Nevertheless, this detection system remains applicable for environments with elevated iron levels, such as acid mine drainage, where Fe(III) concentrations can range from 10 to 2760 mg/L [46], [47], [48]. A summary of the analytical performance parameters is provided in Table 3.

TABLE III. Analytical performance summary for Fe(III) detection using the hue (H) parameter (n=3).

Regression equation	$H = 2.07C + 220.87$
Correlation coefficient ( $R^2$ )	0.9837
Linear Range	1-5 mM
Slope ± SD (°mM)	$2.07 \pm 0.05$
Intercept ± SD (°)	$220.87 \pm 0.25$
$RSD_{slope}$	2.79%
LoD	0.948 mM
LoQ	2.875 mM

One limitation of using hue (H) as the analytical parameter in color-based detection lies in its discrete nature. In most practical applications, particularly those involving smartphone-based image processing, hue is represented as an integer within the 0-360° range, corresponding to positions on the color wheel [49]. In the case of carbon quantum dots, the observable fluorescence color changes typically occur within a narrow hue range, primarily from cyan to blue (approximately 180-240°) [50]. This restricted range, coupled with the lack of decimal precision, limits the method’s ability to resolve subtle changes in analyte concentration. Unlike spectrophotometric or electrochemical measurements, which allow for continuous, high-resolution data, hue-based

detection is constrained by its digital format. As a result, these limitations can reduce the method's resolution and sensitivity, particularly when detecting low-level variations in Fe(III) concentration.

The developed sensing system was further evaluated using real-world samples to assess its applicability (Table 4). Tap water samples were spiked with known amounts of Fe(III) ions, and the recovery values were calculated. The recoveries were considerably higher than the acceptable range of 80–120%, indicating the presence of significant interference and/or matrix effects. Tap water typically contains residual metal ions, oxidizing agents, and exhibits variable pH, which can influence the complexation, quenching, or aggregation processes, altering the hue response [51]. These results confirm that the tap-water matrix can significantly enhance the apparent signal, leading to overestimation of Fe(III) concentration.

TABLE IV. Determination of Fe(III) concentration in tap water (n=3).

Spiked amount (mM)	Amount found (mM)	Recovery (%)
1	2.84 ± 0.34	284.51%
3	5.59 ± 0.34	186.34%
5	15.20 ± 0.34	303.96%

#### 4. CONCLUSIONS

Nitrogen-doped carbon quantum dots (N-CQDs) were successfully synthesized from banana peel waste via a hydrothermal method using urea as a nitrogen source. FTIR and optical analyses confirmed the presence of hydroxyl, carbonyl, and amine functional groups, with a characteristic absorption peak at 304 nm and blue fluorescence emission at 465 nm under 392 nm excitation. The N-CQDs exhibited selective fluorescence quenching in response to Fe(III), accompanied by a measurable shift in hue (H). A strong linear correlation was observed between hue and Fe(III) concentration ( $R^2 = 0.9837$ ), supporting their potential as low-cost, portable probes for Fe(III) detection. While the  $R^2$  value does not meet the ideal threshold of 0.99 typically required for quantitative instrumental analysis, it demonstrates sufficient linearity for preliminary analytical applications.

#### References

- [1] V. Masindi and K. L. Muedi, "Environmental contamination by heavy metals," *Heavy metals*, vol. 10, no. 4, pp. 115–133, 2018.
- [2] Y. Bagbi, A. Pandey, and P. R. Solanki, "Electrospun nanofibrous filtration membranes for heavy metals and dye removal," in *Nanoscale materials in water purification*, Elsevier, 2019, pp. 275–288.
- [3] V. Singh *et al.*, "Toxic heavy metal ions contamination in water and their sustainable reduction by eco-friendly methods: isotherms, thermodynamics and kinetics study," *Sci Rep*, vol. 14, no. 1, p. 7595, 2024.
- [4] G. Prayoga, B. A. Utomo, and H. Effendi, "Heavy Metals Contamination and Water Quality Parameter Conditions in Jatiluhur Reservoir, West Java, Indonesia," *Biotropia (Bogor)*, vol. 29, no. 1, 2022.
- [5] L. N. Fadlillah, S. Utami, A. A. Rachmawati, G. D. Jayanto, and M. Widyastuti, "Ecological risk and source identifications of heavy metals contamination in the water and surface sediments from anthropogenic impacts of urban river, Indonesia," *Heliyon*, vol. 9, no. 4, 2023.
- [6] A. Ahmed, A. Singh, B. Padha, A. K. Sundramoorthy, A. Tomar, and S. Arya, "UV–vis spectroscopic method for detection and removal of heavy metal ions in water using Ag doped ZnO nanoparticles," *Chemosphere*, vol. 303, p. 135208, 2022, doi: <https://doi.org/10.1016/j.chemosphere.2022.135208>.
- [7] X.-Y. Zhang *et al.*, "Nitrogen and sulfur co-doped carbon dots with bright fluorescence for intracellular detection of iron ion and thiol," *J Colloid Interface Sci*, vol. 611, pp. 255–264, 2022, doi: <https://doi.org/10.1016/j.jcis.2021.12.069>.



- [8] M. Nagaraj *et al.*, "Detection of Fe<sup>3+</sup> ions in aqueous environment using fluorescent carbon quantum dots synthesized from endosperm of *Borassus flabellifer*," *Environ Res*, vol. 212, p. 113273, 2022.
- [9] Z. Lu *et al.*, "Smartphone-integrated multi-color ratiometric fluorescence portable optical device based on deep learning for visual monitoring of Cu<sup>2+</sup> and thiram," *Chemical Engineering Journal*, vol. 439, p. 135686, 2022, doi: <https://doi.org/10.1016/j.cej.2022.135686>.
- [10] Z. Gerdan, Y. Saylan, and A. Denizli, "Recent advances of optical sensors for copper ion detection," *Micromachines (Basel)*, vol. 13, no. 8, p. 1298, 2022.
- [11] G. M. Khairy, A. S. Amin, S. M. N. Moalla, A. Medhat, and N. Hassan, "Fluorescence determination of Fe (III) in drinking water using a new fluorescence chemosensor," *RSC Adv*, vol. 12, no. 42, pp. 27679–27686, 2022.
- [12] S. Sharma and P. Chowdhury, "Urea-Based Carbon Quantum Dots for Recognition of Fe<sup>3+</sup> by Fluorescence Quenching and Pb<sup>2+</sup> by Fluorescence Enhancement," *Chempluschem*, vol. 90, no. 6, p. e202400715, 2025.
- [13] A. H. Alshatteri and K. M. Omer, "Smartphone-based fluorescence detection of bilirubin using yellow emissive carbon dots," *Analytical Methods*, vol. 14, no. 17, pp. 1730–1738, 2022.
- [14] S. Phetduang, K. Ngamdee, C. Surawanitkun, X.-K. Ren, and W. Ngeontae, "A portable fluorescence detection device based on a smartphone employing carbon nanodots for Mn<sup>2+</sup> sensing," *Analytical Methods*, vol. 16, no. 14, pp. 2101–2110, 2024.
- [15] C. Dong *et al.*, "High-performance colorimetric detection of thiosulfate by using silver nanoparticles for smartphone-based analysis," *ACS Sens*, vol. 2, no. 8, pp. 1152–1159, 2017.
- [16] A. Hakonen and J. E. Beves, "Hue parameter fluorescence identification of edible oils with a smartphone," *ACS Sens*, vol. 3, no. 10, pp. 2061–2065, 2018.
- [17] E. A. Tarim and H. C. Tekin, "Colorimetric detection of serum creatinine on a miniaturized platform using hue-saturation-value space analysis," *Sci Rep*, vol. 14, no. 1, p. 19441, 2024.
- [18] N. A. Hafez, E. Fadl, S. Ebrahim, M. Soliman, and A. Shokry, "Fluorescent cerium doped carbon quantum dots for detection of ferric ions," *Ceram Int*, 2025.
- [19] R. Zhang and W. Chen, "Nitrogen-doped carbon quantum dots: Facile synthesis and application as a 'turn-off' fluorescent probe for detection of Hg<sup>2+</sup> ions," *Biosens Bioelectron*, vol. 55, pp. 83–90, 2014.
- [20] H. Qi *et al.*, "Biomass-derived nitrogen-doped carbon quantum dots: highly selective fluorescent probe for detecting Fe<sup>3+</sup> ions and tetracyclines," *J Colloid Interface Sci*, vol. 539, pp. 332–341, 2019.
- [21] R. Liu, Y. Zhang, Y. Piao, and L.-Y. Meng, "Development of nitrogen-doped carbon quantum dots as fluorescent probes for highly selective and sensitive detection of the heavy-ion Fe<sup>3+</sup>," *Carbon Letters*, vol. 31, no. 4, pp. 821–829, 2021.
- [22] Y. Zhang *et al.*, "Highly fluorescent nitrogen and boron doped carbon quantum dots for selective and sensitive detection of Fe<sup>3+</sup>," *J Mater Chem B*, vol. 9, no. 23, pp. 4654–4662, 2021.
- [23] M. S. Ali, N. Bhunia, M. S. Ali, S. Karmakar, P. Mukherjee, and D. Chattopadhyay, "Fluorescent N-doped carbon quantum dots: A selective detection of Fe<sup>3+</sup> and understanding its mechanism," *Chem Phys Lett*, vol. 825, p. 140574, 2023.
- [24] A. Tadesse, M. Hagos, D. RamaDevi, K. Basavaiah, and N. Belachew, "Fluorescent-nitrogen-doped carbon quantum dots derived from citrus lemon juice: green synthesis, mercury (II) ion sensing, and live cell imaging," *ACS Omega*, vol. 5, no. 8, pp. 3889–3898, 2020.
- [25] Y. Zhu, L. Yan, M. Xu, Y. Li, X. Song, and L. Yin, "Difference between ammonia and urea on nitrogen doping of graphene quantum dots," *Colloids Surf A Physicochem Eng Asp*, vol. 610, p. 125703, 2021, doi: <https://doi.org/10.1016/j.colsurfa.2020.125703>.

- [26] N. A. Qandeel, A. A. El-Masry, M. Eid, M. A. Moustafa, and R. El-Shaheny, "Fast one-pot microwave-assisted green synthesis of highly fluorescent plant-inspired S,N-self-doped carbon quantum dots as a sensitive probe for the antiviral drug nitazoxanide and hemoglobin," *Anal Chim Acta*, vol. 1237, p. 340592, 2023, doi: <https://doi.org/10.1016/j.aca.2022.340592>.
- [27] S. F. El-Malla, E. A. Elshenawy, S. F. Hammad, and F. R. Mansour, "Rapid microwave synthesis of N,S-doped carbon quantum dots as a novel turn off-on sensor for label-free determination of copper and etidronate disodium," *Anal Chim Acta*, vol. 1197, p. 339491, 2022, doi: <https://doi.org/10.1016/j.aca.2022.339491>.
- [28] S. M. A. Pontes *et al.*, "One-pot solvothermal synthesis of full-color carbon quantum dots for application in light emitting diodes," *Nano-Structures & Nano-Objects*, vol. 32, p. 100917, 2022.
- [29] Z. Pang *et al.*, "Efficient ethanol solvothermal synthesis of high-performance nitrogen-doped carbon quantum dots from lignin for metal ion nanosensing and cell imaging," *Ind Crops Prod*, vol. 183, p. 114957, 2022.
- [30] T. Happi Emaga, R. H. Andrianaivo, B. Wathélet, J. T. Tchango, and M. Paquot, "Effects of the stage of maturation and varieties on the chemical composition of banana and plantain peels," *Food Chem*, vol. 103, no. 2, pp. 590–600, 2007, doi: <https://doi.org/10.1016/j.foodchem.2006.09.006>.
- [31] R. Atchudan, T. N. Jebakumar Immanuel Edison, M. Shanmugam, S. Perumal, T. Somanathan, and Y. R. Lee, "Sustainable synthesis of carbon quantum dots from banana peel waste using hydrothermal process for in vivo bioimaging," *Physica E Low Dimens Syst Nanostruct*, vol. 126, p. 114417, 2021, doi: <https://doi.org/10.1016/j.physe.2020.114417>.
- [32] H.-L. Yang *et al.*, "Carbon quantum dots: Preparation, optical properties, and biomedical applications," *Mater Today Adv*, vol. 18, p. 100376, 2023, doi: <https://doi.org/10.1016/j.mtadv.2023.100376>.
- [33] M. Wu *et al.*, "Preparation of functionalized water-soluble photoluminescent carbon quantum dots from petroleum coke," *Carbon N Y*, vol. 78, pp. 480–489, 2014, doi: [10.1016/j.carbon.2014.07.029](https://doi.org/10.1016/j.carbon.2014.07.029).
- [34] X. Deng, Y. Feng, H. Li, Z. Du, Q. Teng, and H. Wang, "N-doped carbon quantum dots as fluorescent probes for highly selective and sensitive detection of Fe<sup>3+</sup> ions," *Particuology*, vol. 41, pp. 94–100, Dec. 2018, doi: [10.1016/j.partic.2017.12.009](https://doi.org/10.1016/j.partic.2017.12.009).
- [35] L. Zhao, Y. Wang, X. Zhao, Y. Deng, and Y. Xia, "Facile synthesis of nitrogen-doped carbon quantum dots with chitosan for fluorescent detection of Fe<sup>3+</sup>," *Polymers (Basel)*, vol. 11, no. 11, p. 1731, 2019.
- [36] M. A. Omary and H. H. Patterson, "Luminescence, theory," 2017.
- [37] T.-Y. Shen, P.-Y. Jia, D.-S. Chen, and L.-N. Wang, "Hydrothermal synthesis of N-doped carbon quantum dots and their application in ion-detection and cell-imaging," *Spectrochim Acta A Mol Biomol Spectrosc*, vol. 248, p. 119282, 2021.
- [38] Q. Zhang *et al.*, "Green synthesis of mustard seeds carbon dots and study on fluorescence quenching mechanism of Fe<sup>3+</sup> ions," *Inorg Chem Commun*, vol. 146, Dec. 2022, doi: [10.1016/j.inoche.2022.110034](https://doi.org/10.1016/j.inoche.2022.110034).
- [39] J. Jia *et al.*, "Highly luminescent N-doped carbon dots from black soya beans for free radical scavenging, Fe<sup>3+</sup> sensing and cellular imaging," *Spectrochim Acta A Mol Biomol Spectrosc*, vol. 211, pp. 363–372, Mar. 2019, doi: [10.1016/j.saa.2018.12.034](https://doi.org/10.1016/j.saa.2018.12.034).
- [40] N. Hashemi and M. H. Mousazadeh, "Preparation of fluorescent nitrogen-doped carbon dots for highly selective on-off detection of Fe<sup>3+</sup> ions in real samples," *Opt Mater (Amst)*, vol. 121, Nov. 2021, doi: [10.1016/j.optmat.2021.111515](https://doi.org/10.1016/j.optmat.2021.111515).
- [41] M. A. Issa, Z. Z. Abidin, S. Sobri, S. A. Rashid, M. A. Mahdi, and N. A. Ibrahim, "Fluorescent recognition of Fe<sup>3+</sup> in acidic environment by enhanced-quantum yield N-doped carbon dots: optimization of variables using central composite design," *Sci Rep*, vol. 10, no. 1, p. 11710, 2020.

- [42] H. Shabbir, E. Csapó, and M. Wojnicki, "Carbon Quantum Dots: The Role of Surface Functional Groups and Proposed Mechanisms for Metal Ion Sensing," Jun. 01, 2023, *MDPI*. doi: 10.3390/inorganics11060262.
- [43] M. Marpongahtun, A. Andriayani, Y. Muis, and S. Gea, "Synthesis of nitrogen-doped carbon dots from nanocrystalline cellulose by pyrolysis method as Hg<sup>2+</sup> detector," *Synthesis (Stuttg)*, vol. 14, no. 1, 2023.
- [44] A. Horta-Velázquez, G. Ramos-Ortiz, and E. Morales-Narváez, "The optimal color space enables advantageous smartphone-based colorimetric sensing," *Biosens Bioelectron*, vol. 273, Apr. 2025, doi: 10.1016/j.bios.2024.117089.
- [45] M. A. Abdel Hamid, M. M. Mabrouk, H. M. Ahmed, B. Samy, and H. A. Batakoushy, "Carbon quantum dots as a sensitive fluorescent probe for quantitation of pregabalin; application to real samples and content uniformity test," *Luminescence*, vol. 37, no. 1, pp. 170–176, 2022.
- [46] Y. G. Wibowo *et al.*, "Highly Efficient Modified Constructed Wetlands Using Waste Materials for Natural Acid Mine Drainage Treatment," *Sustainability (Switzerland)*, vol. 15, no. 20, Oct. 2023, doi: 10.3390/su152014869.
- [47] G. Kaur, S. J. Couperthwaite, B. W. Hatton-Jones, and G. J. Millar, "Alternative neutralisation materials for acid mine drainage treatment," *Journal of Water Process Engineering*, vol. 22, pp. 46–58, Apr. 2018, doi: 10.1016/j.jwpe.2018.01.004.
- [48] J. S. España, E. L. Pamo, E. Santofimia, O. Aduvire, J. Reyes, and D. Baretino, "Acid mine drainage in the Iberian Pyrite Belt (Odiel river watershed, Huelva, SW Spain): Geochemistry, mineralogy and environmental implications," *Applied Geochemistry*, vol. 20, no. 7, pp. 1320–1356, Jul. 2005, doi: 10.1016/j.apgeochem.2005.01.011.
- [49] A. A. Abdella and E. A. Elshenawy, "A spatial hue smartphone-based colorimetric detection and discrimination of carmine and carminic acid in food products based on differential adsorptivity," *Talanta*, vol. 282, Jan. 2025, doi: 10.1016/j.talanta.2024.127053.
- [50] L. Shuhua and G. Gaizhi, "The application of improved HSV color space model in image processing," in *2010 2nd International Conference on Future Computer and Communication*, 2010, pp. V2-10-V2-13. doi: 10.1109/ICFCC.2010.5497299.
- [51] X. Yan *et al.*, "Carbon Quantum Dot-Incorporated Chitosan Hydrogel for Selective Sensing of Hg<sup>2+</sup> Ions: Synthesis, Characterization, and Density Functional Theory Calculation," *ACS Omega*, vol. 6, no. 36, pp. 23504–23514, Sep. 2021, doi: 10.1021/acsomega.1c03557.